WILEY VCH

RESEARCH ARTICLE

Reversible Redox Probes to Determine Band-Edge Locations and Dopant Concentrations of Nano-TiO_2 Thin-Films: Settling the Mott-Schottky Conundrum

Divyansh Anil Khurana, Nina Plankensteiner, Bart Vermang, Philippe M. Vereecken*

[a] D. A. Khurana, Dr. N. Plankensteiner, Prof. dr. B. Vermang, Prof. dr. P. M. Vereecken
imec Leuven
Kapeldreef 75, 3001 Leuven (Belgium)
E-mail: philippe.vereecken@imec.be

[b] D. A. Khurana, Dr. N. Plankensteiner, Prof. dr. B. Vermang, Prof. dr. P. M. Vereecken
EnergyVille
Thor Park 8320, 3600 Genk (Belgium)

[c] D. A. Khurana, Dr. N. Plankensteiner, Prof. dr. P. M. Vereecken
cMACS, Department for Microbial and Molecular Systems (M2S)
KU Leuven
Celestijnenlaan 200F, 3001 Leuven (Belgium)

[d] Prof. dr. B. Vermang
imo-imomec
Hasselt University
Martelarenlaan 42, 3500 Hasselt (Belgium)

Supporting information (SI) for this article is given via a link at the end of the document.

Abstract: Knowing the exact location of the semiconductor band-edges is key for mechanistic insights into their use for water and CO_2 photo/electrocatalysis. In this regard, a reliable strategy for nano-semiconductors did not exist yet. We demonstrate the use of reversible redox probes on nano-semiconductor electrodes to determine their band-edge locations in aqueous solutions. Rectifying current-potential (i-U) characteristics with the high work function (i.e. more positive formal potential) $Fe(CN)_6^{3-}/Fe(CN)_6^{4-}$ redox couple yielded the exact flatband potential at various pH whereas the reversible i-U characteristics with the low work function (i.e. more negative formal potential) $Ru(NH_3)_6^{3+}/Ru(NH_3)_6^{2+}$ redox couple provided the conduction band-edge location and dopant concentration for a 30nm thin-film n-TiO_2. The methodology can be extended to other nano-semiconductors and serves as an alternative to and goes beyond the capabilities of the Mott-Schottky procedure for bulk semiconductor electrodes.

Introduction

Electricity from renewables can be used to split water to generate green H_2 and to electro-reduce CO_2 to formic acid, methanol, ethylene, etc. for green feedstock to the chemical industry or use as e-fuels.[1] Semiconductors can be employed both as electro- and photo-catalysts in this regard.[2–5] Light absorption to yield electron and hole pairs that could be separated by an intrinsic or extrinsic electric field, and used in separate reduction and oxidation reactions gives the ability for direct solar to chemical conversion. Even though this warrants special inclination towards the field of semiconductor (photo-)electrochemistry from people of diverse scientific backgrounds, fundamental insights into mechanistic pathways are often still lacking. One such example is when determining band-edge locations of these semiconductor catalysts in solution. Mott-Schottky measurement can be used to determine the flatband potential and estimate the dopant concentration for bulk semiconductors. In essence, the capacitance associated with the semiconductor's depletion layer width is determined by electrochemical impedance spectroscopy technique. A change in the electrode potential (U) results in a change of depletion width (Fig. 1B) which is measured via its capacitance (C_{sc}) and leads to the flatband potential (U_{fb}) and dopant concentration (N_D) of the bulk semiconductor electrodes via the well-known Mott-Schottky relationship.[6]

$$C_{SC}^{-2} = \frac{2}{qN_D\epsilon_0\epsilon_{sc}}\left(U - U_{fb} - \frac{kT}{q}\right) \quad (1)$$

But the fact that nano-semiconductors have dimensions which are often much smaller than a typical depletion layer thickness for moderate doping, means that they are fully depleted by a few milli-volts of applied potential. Hence, the Mott-Schottky relationship

cannot be used for such nanoscale semiconductor electrodes as the boundary condition of potential dependent depletion layer capacitance is not valid. Depending upon the relative capacitances of the depleted semiconductor and the Helmholtz layer, varying potential across the nano-semiconductor/solution interface instead corresponds to one of the two possible scenarios wherein the potential may drop across the Helmholtz layer (Fig. 1C) or across the depleted semiconductor (Fig. 1D).

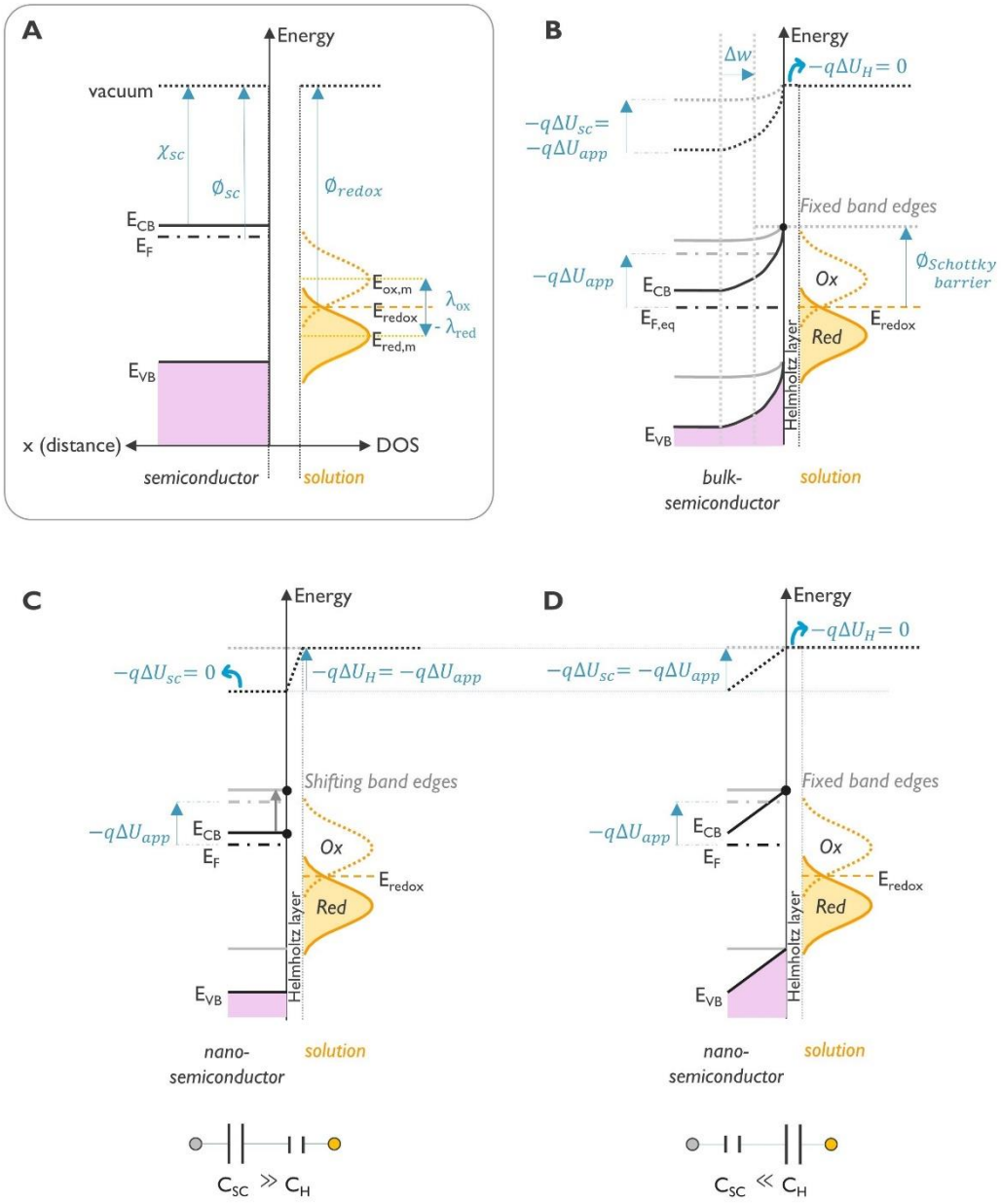

Figure 1. Semiconductor/solution contacts. (A) Electron affinity (χ_{sc}), work function ($\emptyset_{sc}$), conduction band-edge minimum (E_{CB}), fermi level (E_F), and valence band-edge maximum (E_{VB}) energies of the semiconductor relative to the solution work function ($\emptyset_{redox}$), solution fermi level (E_{redox}), most probable oxidant energy state ($E_{ox,m}$), most probable reductant energy state ($E_{red,m}$), and the rearrangement energies for the oxidant and reductant (λ_{ox} and λ_{red} respectively), before contact. (B) Formation of a Schottky barrier ($\emptyset_{Schottky-barrier}$) and the potential dependent depletion (w) across a bulk-semiconductor on contact with a high work function solution; with ΔU_{sc}, ΔU_H being the changes in potential drop across the semiconductor and the Helmholtz layer respectively with a change in applied potential (ΔU_{app}). (C) Fully depleted nano-semiconductor with a capacitance (C_{SC}; SC indicating the semiconductor) higher than the capacitance of the electrical double layer (C_H; H indicating the Helmholtz layer) causes the band edges to shift on application of a varying potential. (D) For a nano-semiconductor with a capacitance (C_{SC}) lower than the Helmholtz capacitance (C_H), the varying potential drops linearly across the semiconductor, as for a dielectric, while the band edges remain fixed.

We demonstrate how reversible redox probes of different formal potentials can be used as electrochemical markers of varying work functions to locate the band edges of a nano-semiconductor electrode in an electrolyte solution. While the strategy has been explored in the past for a more qualitative analysis,[7–10] for the first time, we were able to exactly quantify the flatband potential and

estimate the conduction band edge location and dopant concentration of a 30nm anatase thin-film n-TiO_2 nano-semiconductor model system. Hence, we have shown that measurements with redox probes for nano-semiconductors provide an alternative to the Mott-Schottky procedure for bulk semiconductors.

Results and Discussion

Electrochemical Impedance Spectroscopy And Mott-Schottky Analysis

Potentiostatic electrochemical impedance spectroscopy (PEIS) was performed on bulk and nano-TiO_2 electrodes in a 3-electrode electrochemical setup to emphasize the difference in behavior of their depletion layers. A 0.5mm thick rutile (100) crystal was used as the bulk electrode and 30nm thin-film of polycrystalline anatase (fig. S1) on TiN-coated Si substrates served as the nano dimension counterpart in a solution of 10mM $K_3Fe(CN)_6$ in 0.2M KCl of pH 6. Nyquist impedance plots of the real and imaginary components of the impedance were obtained at potentials between +2V and -1V vs Ag/AgCl (fig. S6). The capacitance of the semiconductor space charge or depletion layer (C_{SC}) can be found from the parallel capacitor (C_P) in the Randles equivalent circuit (inset Fig. 2) in the case that an applied potential difference effectively drops over this depletion layer. The inverse of the capacitance squared (C_P^{-2}) at all the applied potentials (U) for both bulk and nano electrodes are shown in figures 2A and 2B respectively. C_P^{-2} for bulk TiO_2 reduced linearly from +2V to 0V, then rapidly dropped to 0 between 0V and -0.2V and remained 0 for U<-0.2V. This is a textbook example of Mott-Schottky analysis for an n-type semiconductor where a linear decrease in C_P^{-2} with decreasing U corresponds to a changing depletion layer width. The slope of the linear fit provides the dopant concentration (N_D=7.6x10^{18} cm^{-3}) while the intercept with U axis results in the flatband potential, U_{fb} = -0.5V vs Ag/AgCl from the Mott-Schottky relationship (Eq. 1).

The drop in C_P^{-2} to zero for -0.2V<U<0V coincides with onset of faradaic current flow in the cyclic voltammogram. At this point, the potential drops also over the Helmholtz layer, including any contribution of surface states, and the measured capacitance, C_p, is no longer that of the semiconductor depletion layer only and thus Mott-Schottky relation cannot be used for these potentials.

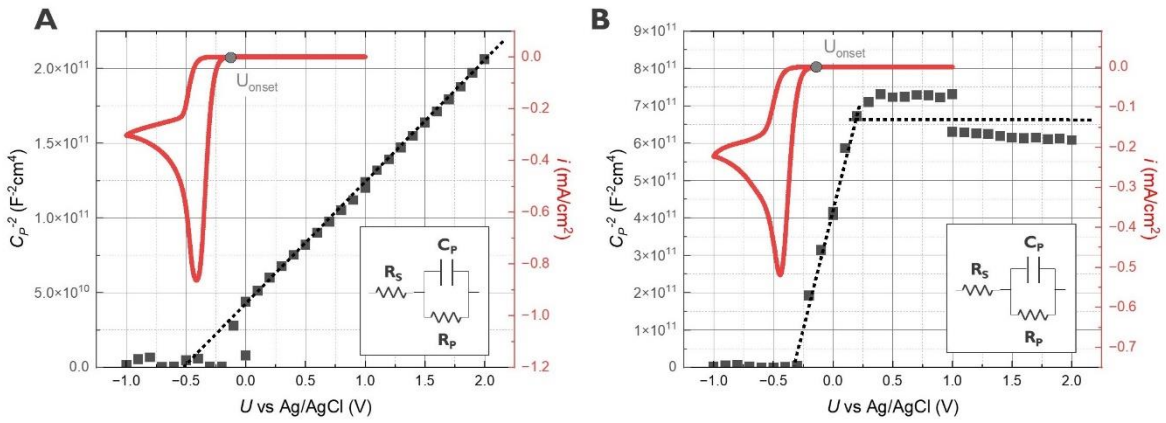

Figure 2. Mott-Schottky plots for bulk and nano-TiO_2 electrodes. C_P^{-2} vs applied potential (U) obtained by fitting a Randles circuit to the Nyquist impedance plots, and cyclic voltammograms for (A) n-type rutile (100) TiO_2 crystal, and (B) n-type thin-film anatase TiO_2 in 10mM $K_3Fe(CN)_6$ (with 0.2M KCl) at pH 6. Note that the jump in C_P^{-2} from 6x10^{11} $F^{-2}cm^4$ to 7x10^{11} $F^{-2}cm^4$ at 1V vs Ag/AgCl is a measurement artefact as a new measurement was started on the same electrode at +1V.

For the nano-TiO_2 film, no linear C_P^{-2} relationship was found in the reverse current potential range, in contrast to the bulk semiconductor. Instead, a constant capacitance (C_P^{-2} ≈ 6.5x10^{11} $F^{-2}cm^4$ or C_P ≈ 1.2 μF/cm^2) for all U>0.2V was found and corresponds to the capacitance of the fully depleted TiO_2 dielectric (C_{TiO2}). In Fig. 2B, C_P^{-2} dropped steeply from +0.2V to -0.3V and reached 0 for U<-0.3V. However, the drop in C_P^{-2} coincides again with the onset of charge flow (forward current) and the applied potential will again drop across the Helmholtz layer and surface states. In contrast to what has been suggested in literature,[11] a linear fit to this apparent linear region for -0.3V<U<+0.2V can therefore not be used to determine flatband and dopant concentration. In fact, only about 27mV would be

needed to build a depletion layer of 30nm[1], which is the entire thickness of the TiO_2 film. The proposed methodology of using reversible redox probes to determine the nano-semiconductor flatband, its conduction band edge position and dopant concentration is shown here as a valid alternative.

Electrochemistry Of Redox Probes On Nano-TiO_2 Electrodes

The methodology to study flatband and band-edge locations of nano-TiO_2 in solution was developed using the formal potentials (U') of reversible redox probes as markers. $FeCl_3$ (U'=+0.50V vs Ag/AgCl), $K_3Fe(CN)_6$ (U'=+0.22V), $Ru(NH_3)_6Cl_3$ (U'= -0.17V), $RuCl_3$ (U'= -0.39V) and $CrCl_3$ (U'= -0.59V) were chosen as their formal potentials spanned the full electrochemical stability window of water (fig. S13). The redox probe formal potentials are then referenced to the vacuum energy level used in physics using Ag/AgCl reduction potential as +0.22V vs the Standard Hydrogen Electrode (SHE) and the reduction potential of SHE known to be +4.44V vs vacuum.[21] As such, we then define the solution work function in eV as the redox probe formal potential referenced to the vacuum level (Fig. 1A). This non-conventional definition of the work function helps us to draw parallels between the semiconductor/electrolyte interface, and the semiconductor/metal contacts in solid-state physics.[12] In analogy, redox probes with high and low work functions were sought to obtain semiconductor/electrolyte contacts that, respectively, show rectifying or reversible current-potential (i-U) characteristics. $[Fe(CN)_6]^{3-/4-}$ ($Ø_{redox}$=4.9 eV) and $[Ru(NH_3)_6]^{3+/2+}$ ($Ø_{redox}$=4.5 eV) (see fig. S13 and table S1) were selected here as the high and low work function probes since they gave the expected current-potential characteristics and are stable in a wide pH range 0 to 14. Their cyclic voltammograms showed the expected reversible reduction and oxidation peaks on a Pt electrode (Fig. 3E). The i-U characteristics for other aqueous redox probes on nano-TiO_2 are treated in a follow-up publication.

Case 1: the nano-TiO_2/$[Fe(CN)_6]^{3-/4-}$ thin-film semiconductor/electrolyte interface

This case is exemplary for redox probes which have a formal potential (U') more positive than the semiconductor flatband potential for all pH, or -qU'<<E_{CB}, where E_{CB} is the semiconductor conduction band edge energy. Hence, this case corresponds to an electrolyte work function, $Ø_{redox}$, being higher than the electron affinity, χ_{sc} of the semiconductor (see Fig. 1A). Figure 3A shows the cyclic voltammogram for the 30nm thin-film nano-TiO_2 electrode in $[Fe(CN)_6]^{3-}$ solutions at selected pH between 0 and 7, and voltammograms at other pH are given in SI (fig. S9). Diffusion-limited cathodic peaks for reduction of $[Fe(CN)_6]^{3-}$ to $[Fe(CN)_6]^{4-}$ were observed for all pH but the onset of reduction and the peaks themselves were shifted to negative potentials. The onset of reduction was in fact more negative than the redox probe formal potential and showed a positive shift with reducing pH. Interestingly, no oxidation currents were seen for pH 6.5, small oxidation currents appeared for pH 3.3 and an even larger oxidation was seen at pH 1.4. While the rectifying diode i-U characteristics at pH 6.5 indicate the existence of a Schottky barrier at the semiconductor/electrolyte interface, the positive shift in onset of reduction towards the redox probe formal potential and appearance of oxidation indicated the lowering of this Schottky barrier with decreasing pH.

The existence of a Schottky barrier at the semiconductor/electrolyte interface and the resulting rectifying diode current-potential behavior is typical for a (bulk) semiconductor. The significant shift in onset potential away from Nernstian equilibrium in bulk semiconductors is related to the fact that the electron capture kinetics is determined by the band bending in the semiconductor.[14] For our nano-TiO_2 thin film semiconductor, a Schottky-like energy barrier between the conduction band edge and the redox probe fermi energy will still exist. However, the bands are considered fully-depleted in the case of nano-sized semiconductors and thus the kinetics or onset potential cannot be explained by thermionic emission of electrons from the semiconductor conduction band.

The capacitance of the fully-depleted nano-TiO_2 dielectric (C_{TiO2} above, in Fig. 2B) was compared to the capacitance of the electrical double layer, indicated by the Helmholtz layer (C_H) at the semiconductor/solution interface (fig. S7). It was found that $C_{TiO2} << C_H$, and hence it is argued that the applied potential more positive of the flatband will entirely drop across the depleted TiO_2 (following the situation depicted in Fig. 1D). The current flow from

[1] The depletion layer width (w) is related to the applied potential difference (ΔU) through the dielectric constant (ϵ_{sc}) and dopant concentration (N_D); $w = \sqrt{\frac{2\epsilon_0\epsilon_{sc}}{qN_D}\Delta U}$. Plugging in $w = 30nm$, ϵ_{sc}= 30 (typical for bulk anatase), and $N_D = 10^{17}cm^{-3}$ (a high estimate for an unintentionally doped TiO_2 thin film) gives $\Delta U = 27mV$.

the nano-semiconductor electrode to the solution can thus commence only when the semiconductor is re-populated with electrons at $U<U_{fb}$. This not only explains the deviation in onset potential from the Nernstian potential, but also makes the onset potential, U_{onset} for reduction in the rectifying i-U characteristics a measure of the nano-semiconductor's flatband potential (U_{fb}). It is hence extremely vital that the onset potential be correctly determined. For our analysis, we compare the faradaic currents for the reduction of $[Fe(CN)_6]^{3-}$ to $[Fe(CN)_6]^{4-}$ to non-faradaic capacitive background currents in 0.2M KCl. The potential at which the current measured in the redox probe solution deviates from the background current determined the onset potential, U_{onset} (fig. S8).

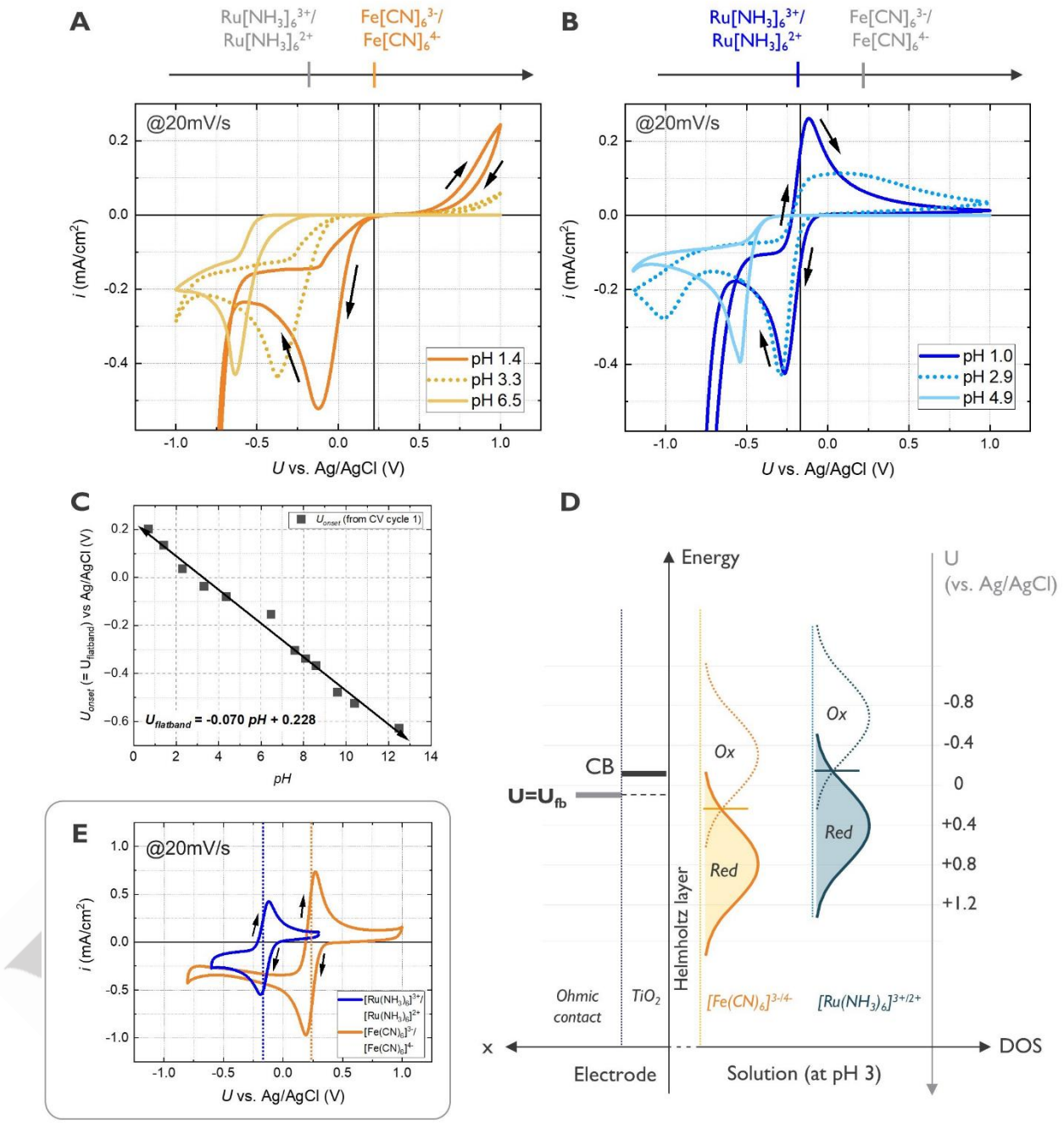

Figure 3. Reversible redox probes measured on nano-TiO_2 electrodes. (A) Rectifying cyclic voltammograms (2nd cycle) for 30nm thin-film nano-TiO_2 electrode with the high-work function solution of 10mM $K_3Fe(CN)_6$ in 0.2M KCl at pH 6.5, 3.3 and 1.4, compared to (B) reversible cyclic voltammograms (2nd cycle) for the nano-TiO_2 electrode at pH 3 and lower in the low-work function solution of 5mM $Ru(NH_3)_6Cl_3$ in 0.2M KCl. The voltammograms were obtained at a scan rate of 20mV/s and the solution pH was adjusted using HCl (pH<7) or KOH (pH>7). (C) Reduction onset potential, $U_{onset}=U_{flatband}$, as a function of solution pH taken from the first cycle in cyclic voltammograms for pristine nano-TiO_2. (D) Flatband and conduction band-edge (CB) position determined for the thin-film nano-TiO_2 electrode at pH 3 relative to the solution energy states. (E) 10mM $K_3Fe(CN)_6$ in 0.2M KCl and 5mM $Ru(NH_3)_6Cl_3$ in 0.2M KCl of as-prepared pH measured on a Pt disk electrode to determine their pH-independent formal potentials.

The onset potentials of the 1st cycle in the voltammogram (fig. S9) are plotted as a function of the solution pH in Figure 3C. A linear relationship with a positive shift in onset potential of 70mV per unit decrease in pH from 12.5 down to 0.7 is found. Intriguingly, bulk semiconductors show a similar shift in their flatband and band edge positions with a change in pH.[15,16] Here, the shift in band edge reflects the change in the potential across the Helmholtz layer because of an associated change in surface charge. The change in surface charge with pH is typically ascribed to a change in the ratio of protonated OH-groups to deprotonated O^- groups on the surface of the semiconductor (fig. S10). A reduced pH leads to more positive surface charge and negative shift in band edge energy with respect to the solution reference. The observation of a 70mV shift in onset potential with pH for our thin-film electrodes is another testament towards the onset potential being a measure of the flatband potential in nano-dimension semiconductors. For pristine nano-TiO_2, the pH dependence of the flatband potential is given by:

$$U_{fb}(pH) = [-0.070\,pH\ +\ 0.228]V\ vs.Ag/AgCl \qquad (2)$$

Case 2: the nano-TiO_2/$[Ru(NH_3)_6]^{3+/2+}$ thin-film semiconductor/electrolyte interface

This case is exemplary for redox probes which have a formal potential close to the semiconductor conduction band edge, i.e. $U' > U_{fb}$ for higher pH and $U' < U_{fb}$ for lower pH. It corresponds to the cases where the electrolyte work function, $\emptyset_{redox}$, is respectively higher and lower than the semiconductor electron affinity, χ_{sc}, for high and low solution pH (Fig. 3D).

Voltammograms for nano-TiO_2 electrodes in $[Ru(NH_3)_6]^{3+}$ solutions of varying pH are given in Figure 3B. For higher solution pH of 4.9, rectifying i-U characteristics were observed where only the reduction current was seen and no oxidation. The onset of reduction was still more negative than the redox probe formal potential for Nernstian behavior. This behavior is similar to what was previously seen for $[Fe(CN)_6]^{3-}$ solution. In fact, the U_{onset} for the rectifying characteristics in $[Ru(NH_3)_6]^{3+/2+}$ macthed the expected U_{onset} ($=U_{fb}$) from Eq. 2 determined using $Fe(CN_6)^{3-/4-}$ (see SI, supplementary text 2). On lowering the pH to 2.9, a broad oxidation peak of $[Ru(NH_3)_6]^{2+}$ to $[Ru(NH_3)_6]^{3+}$ appeared in addition to the reduction peak and hence the start of a reversible behavior of the $[Ru(NH_3)_6]^{3+/2+}$ probe. This again points towards the repositioning of the semiconductor band edges with reducing pH and lowering of the Schottky barrier at the semiconductor/electrolyte interface. The Schottky barrier in fact must disappear and the nano-semiconductor band edge overlaps with both the reductant and oxidant states in solution for the reversible behavior of the redox probe to be seen. This makes the redox probe formal potential a measure of the semiconductor conduction band edge at pH ~3 (see SI). On further reducing the pH to 1, the reversible oxidation peak became sharper and the voltammogram on nano-TiO_2 now looks very similar to those measured on a Pt electrode (see Fig. 3E). The average of the cathodic and anodic peak potentials in this case is -0.17V vs Ag/AgCl and matches very closely with the formal potential for $[Ru(NH_3)_6]^{3+/2+}$ determined on Pt (fig. S16). This confirms that a Schottky barrier is no longer present at the semiconductor/electrolyte interface at pH 1 and the application of potential leads to the shift of the semiconductor band edges about the solution fermi level similar to how the fermi level does for a metal electrode. The electrons can now flow across the interface in either direction showing the reversible nature of the redox probe. Knowing the conduction band edge position at pH 3 from $U'_{Ru(NH3)6}$ and since it must shift with pH similar to the semiconductor flatband potential, we determine the position of the nano-TiO_2 conduction band edge (U_{CB}),

$$U_{CB}(pH)\ =\ -0.17\ +\ 0.070(3-pH)\ V\ vs.Ag/AgCl \qquad (3)$$

It is assumed that the semiconductor band edge positions and flatband only depend on the solution pH, thus remaining the same in both $[Fe(CN)_6]^{3-/4-}$ and $[Ru(NH_3)_6]^{3+/2+}$ solutions of same pH. Using the positions determined for U_{CB} using $[Ru(NH_3)_6]^{3+/2+}$ and for U_{fb} using $[Fe(CN)_6]^{3-/4-}$ at pH 3, we then calculate,

$$\begin{aligned} E_{CB} - E_F\ &=\ -\,q\left[U_{CB} - U_{fb}\right] \qquad (4)\\ &=\ -[(-0.17) - (0.018)]eV\\ &=\ 0.19\ eV \end{aligned}$$

for n-type nano-TiO_2 in contact with an aqueous solution (see Fig. 3D).

The energy difference between the conduction band and the fermi level at flatband ($E_{CB} - E_{F,fb}$) further relates to the dopant concentration (N_D) for an n-type semiconductor,

$$N_D = N_C\ exp\left(-\frac{E_{CB} - E_{F,fb}}{k_B T}\right) \qquad (5)$$

where N_C is the electronic density of states at the conduction band edge, k_B is the Boltzmann's constant ant T is the temperature. N_C is further related to the electron effective mass (m_e^*) in the semiconductor,

$$N_C = 2\left(\frac{2\pi m_e^* k_B T}{h^2}\right)^{3/2} \qquad (6)$$

where h is the Planck's constant. By assuming a typical bulk anatase electron effective mass, $m_e^* = 0.1 m_e$ determined by density function theory,[17] we obtain,

$$N_C = 8\ \times\ 10^{17}\ cm^{-3} \qquad (7)$$

Utilizing $N_C = 8 \times 10^{17}\ cm^{-3}$ and $E_{CB} - E_F = 0.19eV$ for the nano-TiO_2 electrode in Eq. 5, where E_{CB} and E_F were determined from cyclic voltammetry measurements with $[Ru(NH_3)_6]^{3+/2+}$ and

$[Fe(CN)_6]^{3-/4-}$, the dopant concentration for the electrode is estimated at[2],

$$N_D = 5 \times 10^{14}\ cm^{-3} \quad (8)$$

Importantly, by combining the information on the variation of the nano-semiconductor electrode's flatband potential with the solution pH and the location of its conduction band edge from two different redox probes (one with rectifying behavior and one with reversible behavior), we were able to determine the dopant concentration of the thin-film semiconductor. Hence, we have shown that measurements with redox probes for nano-semiconductors do provide an alternative to the Mott-Schottky procedure for bulk semiconductors.

Interpretation: Energy Band Diagrams For Nano-TiO_2 In Aqueous Solutions

Equivalent circuits of resistors and capacitors are used to represent the different components of the nano-TiO_2 electrode (fig. S11), namely (i) the TiN/TiO_2 interface, (ii) TiO_2, and (iii) the Helmholtz layer at the TiO_2/solution interface. Investigating potential distribution over these components is essential to represent the measured i-U characteristics (Fig. 3A) with energy band diagrams for the nano-semiconductor/solution interface. To verify the electrical characteristics of the TiN/TiO_2 interface, metal contact pads of Al (Ohmic) and Au (Schottky) were sputtered on top of the TiO_2 films (fig. S12a). Current-voltage curves (fig. S12b) confirmed pure resistive or Ohmic contact for the TiN/TiO_2/Al and thus TiN/TiO_2 contact, with a negligible iR drop to the i-U characteristics (see SI, supplemnetary text 4). From impedance spectroscopy with varying potentials between the Au top contact and the TiN bottom contact, also any potential drop contribution over the TiN/TiO_2 interface could be discerned (fig. S12c). From prior discussions on the nano-TiO_2 and Helmholtz layer capacitances, we further know that an applied potential only drops across the TiO_2 dielectric for $U>U_{fb}$, and across the Helmholtz layer for $U<U_{fb}$.

Knowing the flatband and the conduction band-edge positions of the nano-TiO_2 electrode, and following the discussions on potential distributions across the different components of the thin-film nano-TiO_2 electrode, the voltammogram in Fig. 3A can be explained through a sequence of band diagrams. Figures 4 A-D show the semiconductor bands for selected potentials more positive and negative of the flatband for our nano-TiO_2 electrode, whilst the band diagrams at other intermediate potentials are given in SI (fig. S17). Rearrangement energies (λ_{ox} and λ_{red}) of ~0.6eV are used for the $[Fe(CN)]_6^{3-}$ and $[Fe(CN)]_6^{4-}$ redox states.[18] Given the large bandgap for anatase nano-TiO_2 thin-film electrodes ($E_g > 3.2eV$)[19] and as the -qU' of the redox probes are close to the conduction band (<400meV), the overlap of the semiconductor valence band states with the redox probe states is negligible. Therefore, only the conduction band of the semiconductor is shown.

[Fig. 4A] Starting from open circuit potential into the forward scan of the cyclic voltammogram (i.e. increasingly more negative potentials) in the potential range where $U > U_{fb}$, the TiO_2 electrode is fully depleted with no electrons at its conduction band edge. Any electron capture associated reduction currents were thus absent. Even though $U < U'_{FeCN6}$, the reduction of $[Fe(CN)_6]^{3-}$ cannot happen ($U > U_{onset}$) as the semiconductor is still depleted of all electrons. The potential drops across the depleted TiO_2 and its conduction band edge remains fixed in energy. [Fig. 4B] At $U = U_{fb}$, the TiO_2 band edge and the surface states close to it become repopulated with electrons available for capture by the $[Fe(CN)_6]^{3-}$ oxidant states which overlap with these semiconductor electronic states[3]. [Fig. 4C] A further decrease in potential ($U < U_{fb}$) sustains charge transfer across the Helmholtz layer causing the applied potential to drop across it. The semiconductor band edges thus move higher up in energy. Note that an accumulation layer will form within nano-TiO_2 for $U < U_{fb}$, and a fraction of the potential also fall across it. But the conduction band edge shifts to higher energies for all $U < U_{fb}$, and hence the bands are shown flat for the sake of simplicity.[20] The continuous flow of charge also gives rise to a diffusion-limited reduction peak in the voltammogram. Scanning towards less negative potentials in the reverse scan of the voltammogram, the band edges shift lower in energy while the current remains diffusion limited. [Fig. 4D] For $U > U_{fb}$ during the reverse scan in the voltammogram, TiO_2 exists in depletion again and no reduction can happen anymore. The conduction band edge remains fixed and the potential drops again over the thin semiconductor, with the

[2] Even though the extracted doping density is well within the range expected for bulk anatase,[23] unfortunately the exact value could not be cross-checked with other physical methods.

[3] Surface-state mediated electron transfer for sustained faradaic (reduction) current flow at a semiconductor electrode, requires its conduction band to be repopulated with electrons. Since nano-semiconductors (unlike in bulk electrodes) are fully-depleted by a few mVs of applied potential, its conduction band will be repopulated with electrons only at $U<U_{fb}$. Hence, $U_{onset} \approx U_{fb}$ for nano-semiconductors even in the presence of surface states (ss). Once $U<U_{fb}$, the conduction band electrons can also populate the ss which contributes to the shift in band edges. Note that in our explanation, the potential drop of ss is included in the potential drop over the Helmholtz layer. In fact, for $U<U_{fb}$, the potential drops entirely over the Helmholtz layer which could be interpreted also as Fermi-level pinning.

reductant states overlapping with the energy bandgap of TiO_2. Electron injection from the $[Fe(CN)_6]^{4-}$ reductant states into the TiO_2 conduction band can hence not occur even for $U > U'_{FeCN6} > U_{fb}$ and thus no anodic current for reversible oxidation of $[Fe(CN)_6]^{4-}$ is observed. This leads to the rectifying behavior in the TiO_2 i-U characteristics.

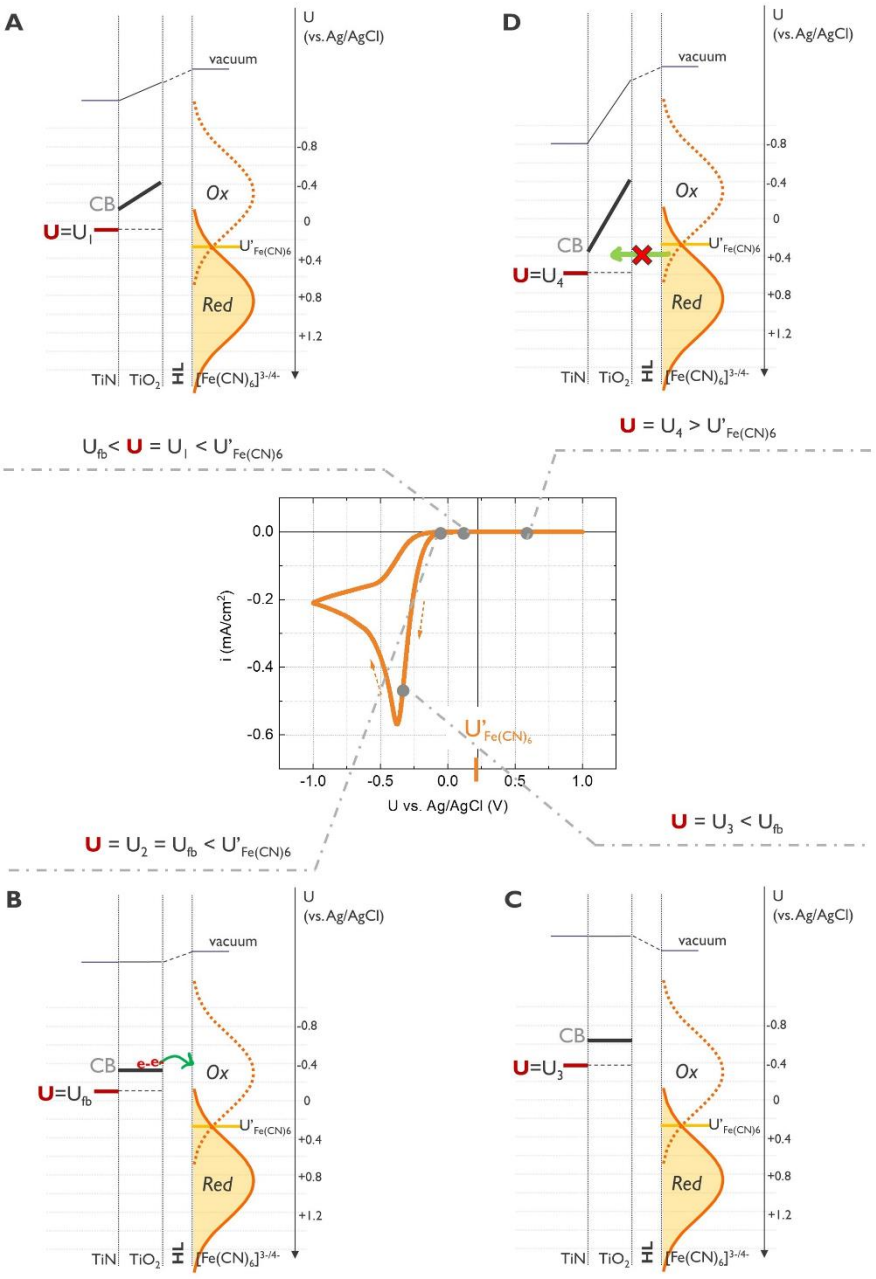

Figure 4. Evolution of the thin-film nano-TiO_2 electrode conduction band. (A-D) Energy band diagrams for the nano-TiO_2 electrode at selected potentials along the rectifying voltammogram obtained in the high work function solution of 10mM $K_3Fe(CN)_6$ in 0.2M KCl at pH 4.5. HL denotes the Helmholtz layer.

A decrease in solution pH increases the number of protons adsorbed on the nano-TiO_2 electrode surface. The associated increase in charge stored across the capacitive Helmholtz layer then increases the potential drop across the Helmholtz layer. The result is that the TiO_2 band edges move to lower energies relative to the solution such that the Schottky barrier at the interface is lowered. The TiO_2 conduction band which had no overlap with the $[Fe(CN)_6]^{4-}$ reductant states previously, has some overlap with the reductant states at a reduced pH (see Figs. 5A-B). This allows for small oxidation currents to flow at larger positive potentials at pH 3.3 (Fig. 3A). (Note: as only the tail of the Gaussian reductant states may overlap with the semiconductor conduction band edge

even at low pH, potentials much larger than the redox probe formal potential are required to allow tunneling of electrons from even lower energy reductant states for appreciable oxidation currents.)

Since the semiconductor flatband potential effectively measures the position of the fermi level at zero band-bending, $E_F = -qU_{fb}$, the absolute fermi level position of the semiconductor could be determined. Utilizing the formal potential for the stable Ag/AgCl reference, $U_{Ag/AgCl}$ = +0.22V vs. SHE, and U_{SHE} = +4.44V vs. vacuum in Eq. 2,[21] the absolute nano-TiO_2 fermi level in aqueous solutions is determined to vary between -4.87eV at pH 0 and -4.45eV at pH 7. This range is in good agreement with the fermi level of our nano-TiO_2 of -4.46eV determined by ultraviolet photoelectron spectroscopy (UPS) in vacuum.[22] This further validates the redox probe methodology to study nano-semiconductor band edges[4].

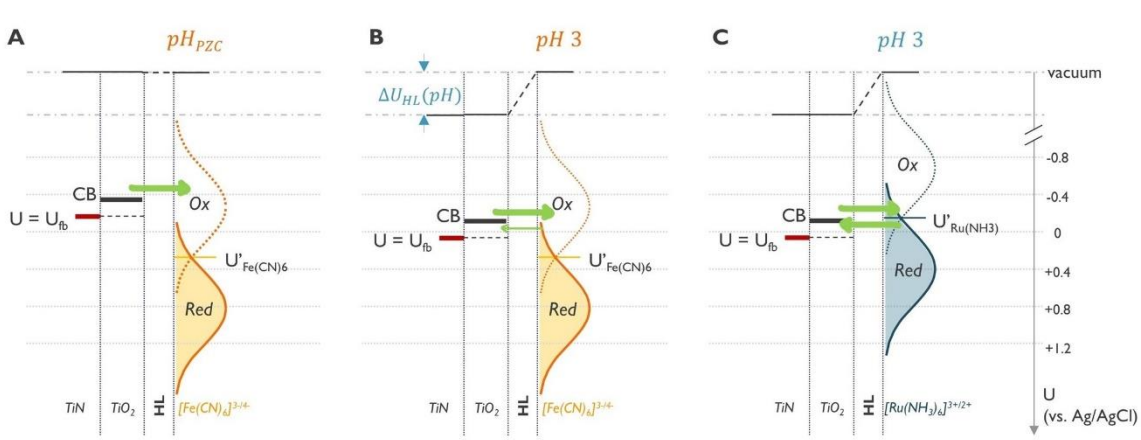

Figure 5. Nano-TiO_2 electrode energy band diagrams at flatband for contact with different solutions. (A) At $U=U_{fb}$ in $Fe(CN)_6^{3-/4-}$ redox probe at pH 6, (B) at $U=U_{fb}$ in $Fe(CN)_6^{3-/4-}$ redox probe at pH 3, and (C) at $U=U_{fb}$ in $Ru(NH_3)_6^{3+/2+}$ redox probe at pH 3. HL denotes the Helmholtz layer and $\Delta U_{HL}(pH)$ denotes the potential difference across it due to the non-zero net surface charge at the TiO_2 electrode. $\Delta U_{HL}(pH)$ becomes zero at the point of zero charge (PZC), when the net surface charge becomes zero, and can be determined as in SI.

In contrast to the rectifying characteristics measured for $[Fe(CN)_6]^{3-/4-}$ at all solution pH of 0.7-12.5, reversible reduction and oxidation currents were measured for the $[Ru(NH_3)_6]^{3+/2+}$ probe with their respective diffusion-limited peaks for a solution pH < 3 (Fig. 3B). More importantly, the potential for onset of reduction was slightly positive and the onset for oxidation slightly negative of the redox probe's formal potential and resembles more the voltammogram measured on Pt. This would mean that in addition to the oxidant $[Ru(NH_3)_6]^{3+}$, a large part of the $[Ru(NH_3)_6]^{2+}$ reductant density of states also overlap with the nano-TiO_2 conduction band edge for electrons to tunnel back to the electrode. The semiconductor conduction band edge hence must exist close to the solution fermi level in energy allowing for easier flow of electrons in both directions across the semiconductor/solution interface (see Fig. 5C). Note that the reversible redox behavior at nano-TiO_2 does not mean it behaves like a metal, as the electron capture and injection processes do not follow Butler-Volmer type kinetics. This is reflected in the average of the peak potentials determined from the reversible voltammograms on nano-TiO_2, which is 30mV more negative than the formal potential measured on Pt (fig. S16). The reversible voltammogram in Fig. 3B could also then be explained through a sequence of nano-TiO_2 band diagrams:

Scanning increasingly negative potentials constitutes the forward scan of the CV. The nano-TiO_2 band edge is repopulated with electrons at U_{fb} = 0.034V vs Ag/AgCl, but no reduction currents are observed at $U=U_{fb}$. This is because even at $U=U_{fb}$, $U>U'_{Ru(NH3)6}$ and the reduction process is thermodynamically prohibited. [Fig. 6A] At $U<U_{fb}$, the applied potential drops across the Helmholtz layer and the conduction band moves higher up in energy. The onset of reduction due to electron capture by the $[Ru(NH_3)_6]^{3+}$ oxidant states is observed as U approaches $U'_{Ru(NH3)6}$. The onset is in fact 50mV positive of the redox probe formal potential measured on the Pt electrode. [Fig. 6B]. On further decrease in potential, the conduction band edge moves to higher energies overlapping with exponentially increasing oxidant density of states (DOS) and results in increasing cathodic currents. As the potential is decreased further, the diffusion-limited cathodic peak is observed.

[4] A comparison to nano-TiO_2 flatband potentials in literature would be untrue. This is because the reported values were either only measured for bulk electrodes or determined via erroneous Mott-Schottky analysis on nano-electrodes.

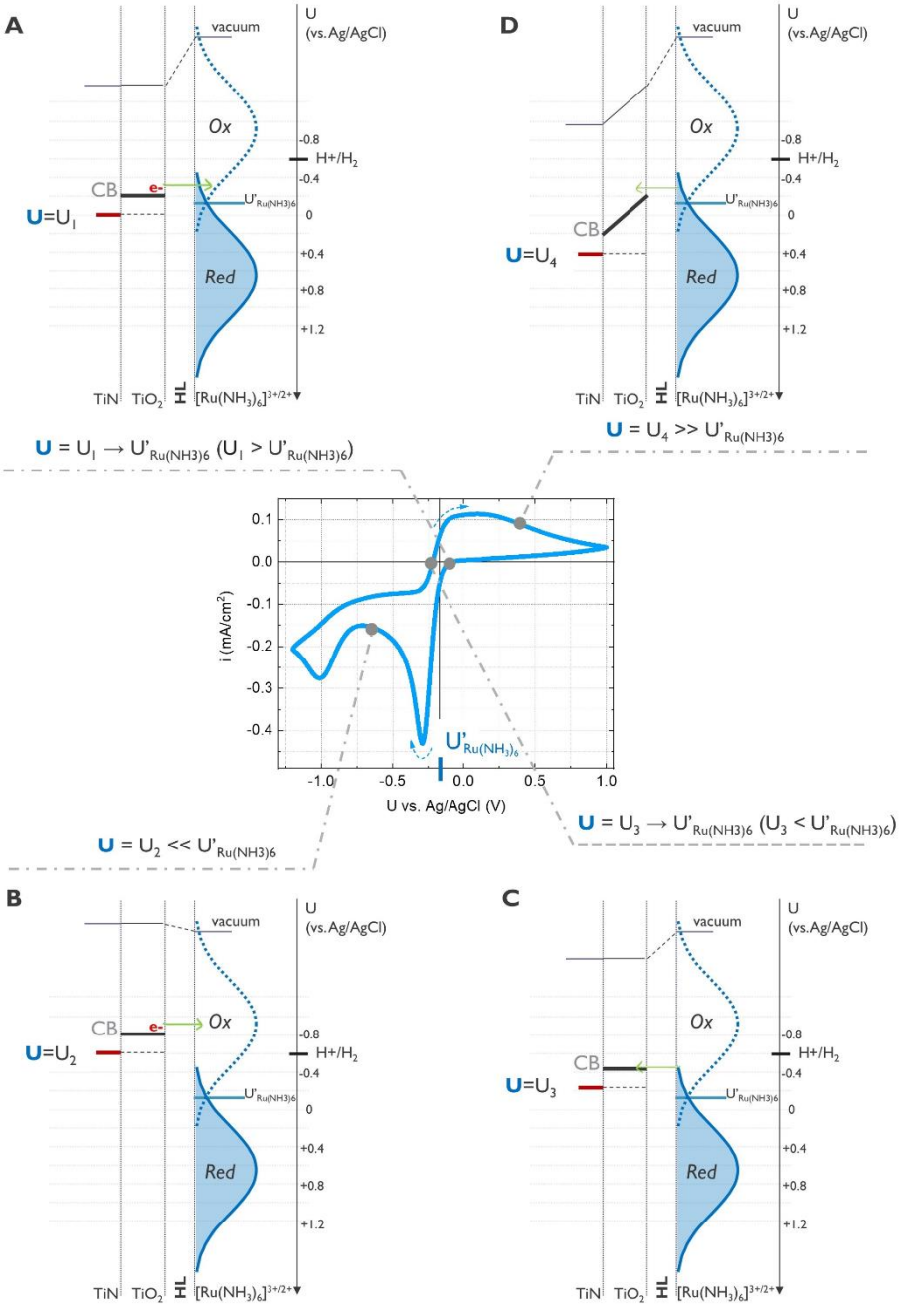

Figure 6. Evolution of the thin-film nano-TiO_2 conduction band. (A-D) Energy band diagrams for the nano-TiO_2 electrode at selected potentials along the reversible voltammogram obtained in the low work function solution of 5mM $Ru(NH_3)_6Cl_3$ in 0.2M KCl at pH 3. HL denotes the Helmholtz layer.

Scanning towards less negative potentials in the reverse scan of the voltammogram, the nano-TiO_2 conduction band edge shifts to lower energies and the current remains diffusion-limited. [Fig. 6C] As U approaches $U'_{Ru(NH3)6}$, the onset of oxidation due to electron injection from the $[Ru(NH_3)_6]^{2+}$ reductant states into the conduction band edge is observed. The onset of oxidation is 50mV negative of the redox probe formal potential. At increasingly positive potentials, the conduction band edge shifts to lower energies such that it overlaps with exponentially increasing reductant DOS, resulting in an initial increase in oxidation currents. [Fig. 6D] With increasingly positive potentials though, and at $U>U_{fb}$, the conduction band edge remains fixed, potential drops across the nano-TiO_2 dielectric, and the electron-injection kinetics become potential independent. The oxidation currents thus did not increase further and in fact saturated. Scanning towards more positive potentials, oxidation currents eventually reach diffusion limitation resulting in a very broad oxidation peak. Scanning towards less positive potentials in the forward scan of the CV, the

conduction band edge remains fixed, and the oxidation currents remain diffusion-limited. At $U=U'_{Ru(NH3)6}$, both reduction and oxidation are possible at the nano-TiO_2 conduction band edge. A more complete sequence of nano-TiO_2 energy band diagrams is given in SI (fig. S18).

Conclusion

This study of nano-semiconductor electrodes with reversible redox probes expands on the known concepts in semiconductor electrochemistry and solves the decades long Mott-Schottky conundrum. We could exactly map the change in nano-semiconductor electrode's flatband with pH, and estimate its conduction band edge position and dopant concentration by analyzing the rectifying and reversible cyclic voltammograms in a high and low work function redox probe solution respectively. However, the study was currently limited to dense thin-film electrode architectures where only the semiconductor/solution interface are measured for the purposes of demonstration. Suggestions are provided in SI under "Recommendations to apply the methodology", to adapt the study for other morphologies and different semiconductors, including those prone to electrochemical corrosion phenomena.

Supporting Information

The authors have cited additional references within the Supporting Information.[13,24,25,26,27,28,29,30,31,32,33,34]

Acknowledgements

The authors acknowledge funding from VLAIO (Flanders Innovation and Entrepreneurship) under the Flanders Industry Innovation Moonshot program for the SYN-CAT (HBC.2020.2614) project.

Competing interests: The authors declare that they have no competing interests.

Data and materials availability: All data needed to evaluate the conclusions and interpretations in this manuscript are present in the main text or the supporting materials. Additional data is available on request to the corresponding author.

Keywords: electrochemistry • energy band diagram • nano-titanium dioxide • redox probes • semiconductors

[1] Z. Yan, J. L. Hitt, J. A. Turner, T. E. Mallouk, *PNAS* **2020**, *117(23)*, 12558–12563.

[2] A. Fujishima, K. Honda, *Nature* **1972**, *238*, 37–38.

[3] T. Inoue, A. Fujishima, S. Konishi, K. Honda, *Nature* **1979**, *277*, 637–638.

[4] K. Sivula, R. van de Krol, *Nat. Rev. Mater.* **2016**, *1*, 15010.

[5] M. Grätzel. *Nature* **2001**, *414*, 338–344.

[6] S.R. Morrison, *Electrochemistry At Semiconductor And Oxidized Metal Electrodes*, Plenum New York, **1980**, p.127.

[7] S. N. Frank, A. J. Bard, *J. Am. Chem. Soc.* **1975**, *97*, *26*, 7427–7433.

[8] L.F. Schneemeyer, M. S. Wrighton, *J. Am. Chem. Soc.* **1979**, *101*, *22*, 6496–6500.

[9] R.A.L. Vanden Berghe, F. Cardon, W.P. Gomes, *Surface Science* **1973**, *39(2)*, 368–384.

[10] L. Kavan, N. Tétreault, T. Moehl, M. Grätzel, *J. Phys. Chem. C* **2014**, *118(30)*, 16408–16418.

[11] R. van de Krol, A. Goossens, J. Schoonman, *J. Electrochem. Soc.* **1997**, *144*, 1723.

[12] L. Michalas, A. Khiat, S. Stathopoulos, T. Prodromakis, *J. Phys. D: Appl. Phys.* **2018**, *51*, 425101.

[13] N. Elgrishi, K. J. Rountree, B. D. McCarthy, E. S. Rountree, T. T. Eisenhart. J. L. Dempsey, *J. Chem. Educ.* **2017**, *95*, 2, 197–206.

[14] W. P. Gomes, F. Cardon, *Progress in Surface Science* **1982**, *12*, 155–216.

[15] S. R. Morrison, *Progress in Surface Science* **1971**, *1(2)*, 105–154.

[16] E. C. Dutoit, F. Cardon, W. P. Gomes, *Ber. Bunsenges. Phys. Chem.* **1976**, *80(6)*, 475–481.

[17] J. Zhang, P. Zhou, J. Liu, J. Yu, *Phys. Chem. Chem. Phys.* **2014**, *16*, 20382–20386.

[18] K. W. Frese Jr, *J. Phys. Chem.* **1981**, 85, 25, 3911–3916.

[19] A. Jolivet, C. Labbé, C. Frilay, O. Debieu, P. Marie, B. Horcholle, F. Lemarié, X. Portier, C. Grygiel, S. Duprey, W. Jadwisienczak, D. Ingram, M. Upadhyay, A. David, A. Fouchet, U. Lüders, J. Cardin, *Applied Surface Science* **2023**, *608*, 155214.

[20] A. Natarajan, G. Oskam, P. C. Searson, *J. Phys. Chem. B* **1998**, 102, 40, 7793–7799

[21] S. Trasatti, *IUPAC, Pure & Appl. Chem.* **1986**, *58(7)*, pp. 955–66.

[22] B. de la Fuente, D. A. Khurana, P. M. Vereecken, A. Hubin, T. Hauffman, *ACS Appl. Mater. Interfaces* **2024**, 16, 37, 49926–49934.

[23] A. Boonchun, P. Reunchan, N. Umezawa, *Phys. Chem. Chem. Phys.* **2016**, *18*, 30040-30046.

[24] L. Hubrechtsen, P. M. Vereecken, *Chem. Mater.* **2022**, *34*, 15, 6753–6768.

[25] S. Moitzheim, S. De Gendt, P.M. Vereecken, *J. Electrochem. Soc.* **2019**, *166*, A1.

[26] S.R. Morrison, *Electrochemistry At Semiconductor And Oxidized Metal Electrodes*, Plenum New York, **1980**, pp.60

[27] M. Morales, M. Risch, *J. Phys. Energy* **2021**, *3*, 034013.

[28] Y. Matsumoto, T. Yoshikawa, E. Sato, *J. Electrochem. Soc.* **1989**, 136, 1389–1391.

[29] M. A. Butler, *J. Appl. Phys.* **1977**, 48, 1914–1920.

[30] G. Horowitz, P. Allongue, H. Cachet, *J. Electrochem. Soc.* **1984**, 131, 2563–2569.

[31] S. M. Ahmed, *Electrochim. Acta* **1982**, 27(6), 707–712.

[32] D. Mandler, A. J. Bard, *Langmuir* **1990**, 6, 9, 1489–1494.

[33] J. L. Weyher, D. H. van Dorp, T. Conard, G. Nowak, I. Levchenko, J. J. Kelly, *J. Phys. Chem. C* **2022**, 126, 1115–1124.

[34] P. M. Vereecken, F. V. Kerchove, W. P. Gomes, *Electrochim. Acta* **1996**, 41(1), 95–107.

Entry for the Table of Contents

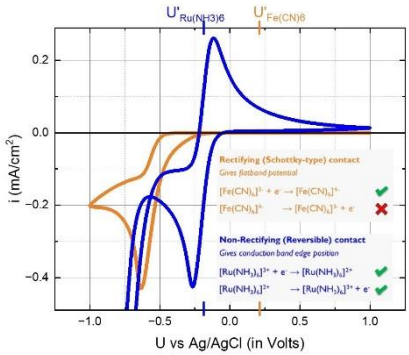

We extend concepts in semiconductor electrochemistry through current-potential measurements for reversible redox active species on a thin-film nano-semiconductor electrode. In the process, we demonstrate a novel but facile methodology to determine a nano-semiconductor electrode's flatband potential, and estimate its conduction band edge position and dopant concentration.

Institute and/or researcher Twitter usernames: @KU_Leuven, @imec_int, @DivAK_30